

## Velocity Measurements in a Mechanical Precessing Jet Flow using Particle Image Velocimetry

K.C. Clayfield, R.M. Kelso, G.M. Schneider, G.J. Nathan

Department of Mechanical Engineering  
 University of Adelaide, Adelaide, South Australia, 5005 AUSTRALIA

### Abstract

The present paper describes instantaneous velocity field data of the non-reacting flow produced by a mechanical precessing jet (MPJ) nozzle at a Reynolds number of 20000. Data are obtained using Particle Image Velocimetry (PIV). The data presented show the first detailed instantaneous measurements of the flow structure generated by the MPJ nozzle. Velocity and vorticity fields show strong consistency with previous point measurements and flow visualisation data. The data show the strong entrainment of the helical MPJ and also suggest that a region of reversed flow exists in the near field. Further work should reveal the details of this complex flow.

### Introduction

The Department of Mechanical Engineering at Adelaide University has been carrying out research into precessing jet technology, used in industrial burners, for over a decade. The flow field produced by PJ nozzles is highly complex. It is generated by a self-excited fluid mechanical instability that occurs following flow through an orifice plate or a smooth contraction with a large sudden expansion into a short cavity [3]. A lip at the exit of the cavity causes the time dependent asymmetric reattachment of the jet-like flow to be deflected as it leaves the cavity. The entire flow then precesses about the axis of the cavity. This configuration is referred to as the “fluidic precessing jet” (FPJ) nozzle [3].

The FPJ nozzle has been patented and commercialised as the GYRO-THERM™ burner, and operates in a number of large scale industrial rotary kilns both within and outside Australia [1]. Experiments in a laboratory furnace have shown the typical maximum time-averaged flame temperature of the PJ flame to be 150°C lower than that of a comparable swirl burner. The NO<sub>x</sub> emissions are reduced by about 50%, while low CO emissions are maintained [1]. However, there are many questions yet to be answered about the mechanisms by which jet precession influences mixing and combustion.

To gain insight into the fluid mechanical processes which result from jet precession, it is advantageous to study the precessing flow under controlled conditions. The precession may be controlled through the use of a “mechanical” precessing jet (MPJ) nozzle, developed by Schneider [12], and shown in figure 1.

The mechanical nozzle produces a jet with known and well defined initial conditions (diameter  $d_e$ , shape, deflection angle  $\phi$ , frequency of precession  $f_p$ , velocity  $u_e$ , jet exit location) that may be varied independently. This allows the MPJ to be compared with simple axial jets. The well-defined, independently variable initial conditions of the MPJ nozzle also allow the exiting jet flow to be characterised by both a Reynolds number,  $Re = u_e d_e / \nu$ , and a Strouhal number of precession,  $St = f_p d_e / u_e$ , which are decoupled from one another. Additionally, the MPJ nozzle allows conditional phase-averaging of the data.

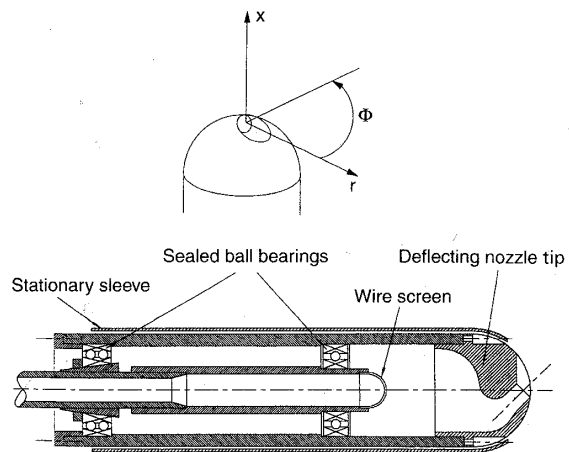


Figure 1. The Mechanical Precessing Jet Nozzle and Coordinate System.

### Background

#### The Importance of the Velocity Field

Investigations by Nathan *et al.* [6], Nobes [8], Schneider [12] and others suggest that large scale turbulent motion may contribute directly to scalar mixing in precessing jet flows, as well as enhancing scalar mixing through the promotion of fine-scale turbulence.

By studying the velocity and concentration fields of the MPJ flow simultaneously, regions of fine and large scale turbulent motion can be identified by the presence of high velocity gradients. These can be compared with regions of high scalar gradient, indicative of scalar mixing. The correlation between the velocity and scalar fields will indicate the effect of the large-scale structures on scalar mixing, and lead to an understanding of the mechanisms driving scalar mixing in precessing flows.

### Previous Studies

Schneider *et al.* [11, 12, 13] conducted the first investigations of the MPJ flow, examining the velocity and pressure fields produced in the near field of the jet (to  $x/d_e = 14$ ). Schneider *et al.* [11, 12] used both hot-wire anemometry and pressure probes to measure the velocity field of the MPJ flow, but definitive three-component velocity measurements were achieved through the use of Laser Doppler Anemometry (LDA). Experiments were performed in air with an MPJ nozzle of exit diameter  $d_e = 10$  mm. Measurements were made in 7 planes, beginning at a distance of 2 nozzle diameters downstream from the nozzle exit plane and then at intervals of 2 nozzle diameters in the axial direction (see figure 2 for co-ordinate system). The velocity profiles of the MPJ flow obtained through this LDA analysis, while providing adequate cross-sections of the flow field, are sparse in the axial direction, and do not extend into the far field of the flow.

Mi *et al.* [2] undertook a study of the mean velocity field of the MPJ, to assess the impact of Strouhal number on mean velocity.

They used hot-wire anemometry to investigate the flow to a downstream distance of  $x/d_e=20$ , and showed that the characteristics of the mean flow are determined predominantly by Strouhal number.

The work of these authors is the primary source of information on the fundamental dynamic behaviour of the non-reacting mechanically precessed jet flow, and is used for comparison with the results obtained in the current investigation.

### PIV Measurements of the FPJ

Limited PIV measurements of the fluidic precessing jet (FPJ) have been performed by Newbold *et al.* [7] and Nobes [9]. These studies highlight some of the difficulties of applying PIV to the complex FPJ flow, but also demonstrate that the PIV technique can be successfully applied to this flow. Such observations are equally applicable to the analogous MPJ flow.

Newbold *et al.* [7] carried out experiments which measured the velocity field to a downstream distance of approximately 30 diameters (with respect to the upstream orifice of the jet). The velocity of the precessing jet flow decays at a much higher rate than in a simple axial, non-precessing jet. Typically, the MPJ flow decays twice as fast as an axial turbulent jet in the first 12 diameters; by a downstream distance of  $x/d_e=6$ , the MPJ flow has decayed to about 29% of its initial value [13]. A similarly rapid decay of mean velocity is exhibited by the flow field of the fluidic precessing jet [5]. This high velocity decay rate presents some practical difficulties when imaging a large region of the flow using the PIV technique. As Newbold *et al.* [7] observed, “there is no suitable pulse separation that produces well separated particle images both where the velocity is highest, at the nozzle exit, and where it is lowest, at the lower edges of the imaged region.”

Newbold *et al.* [7] used a time between laser pulses,  $\Delta t$ , which gave a maximum determinable velocity that was an order of magnitude smaller than the mean jet exit velocity. However, the rapid decay in jet velocity meant that good vectors were obtained for the majority of the imaged area. It was apparent that motion was predominantly in the axial direction, and some eddy-like motion was evident.

A field of view of the FPJ of approximately 12 jet exit diameters in length was imaged by Nobes [9]. This field, however, was a composite array of 16 (4 x 4) smaller images. Taking PIV measurements of the flow field separately over a number of different regions allowed the time between laser pulses,  $\Delta t$ , used for each region to be optimised to the mean velocity of each particular region. In the field of view immediately downstream from the jet exit plane, two values of  $\Delta t$  were used; a  $\Delta t$  eight times greater than that required to give optimal images of the jet was used to capture the low speed surrounding co-flow. These measurements gave very good resolution of flow characteristics.

### The PIV Technique – 3D Errors

One of the disadvantages of PIV is that it is only capable of measuring velocity in the plane of the light sheet; the out-of-plane velocity component is lost, while the in-plane components are affected by an unrecoverable error due to perspective [10]. For highly three-dimensional flows this can lead to substantial measurement errors.

The flow field of the MPJ is certainly three-dimensional, however, Schneider's [12] measurements of the near field velocity indicate that the axial component is the dominant

component of velocity. Hence it is reasonable to conclude that, while there will be some errors due to out-of-plane motion in the velocity field of the MPJ flow, neglecting them will not adversely affect interpretation of the flow field. The PIV results of Nobes [9] support this conclusion, giving good resolution of flow characteristics of the FPJ, which generates a three-dimensional flow similar to that of the MPJ.

### Experimental Setup

Experiments were performed in a wind tunnel, 0.5m x 0.55m in cross-section and 0.8m in height. An MPJ with a diameter of 10mm and a deflection angle of  $45^\circ$  was used, with a mean jet exit velocity of 30m/s and a Reynolds number of 20000. Images were taken at  $f_p=0$  and 10Hz ( $St=0.003$ ). The mechanical precessing jet was driven by an electric motor, controlled by an ABB ASC200 variable frequency driver.

Both the jet and the very low velocity co-flow were seeded with olive oil droplets with a mean diameter of  $1\mu m$ . This seed particle diameter is considered sufficient to follow gaseous flows even at very high velocities [10]. The seeding for the main jet was produced by a TSI six jet atomiser. Co-flow seeding was produced by a Laskin nozzle particle generator manufactured in-house.

The laser used was a 400mJ/pulse Quantel Brilliant Twins Double Pulse Nd:YAG laser, frequency-doubled to 532nm. The timing of the laser pulses generated by this system was controlled by external triggering of both the flash-lamps and Q-switches of each laser. External triggering was achieved using a Quantel Twins DPS01 timing box. Images were collected with the time between laser pulses,  $\Delta t$ , initially set to  $50\mu s$  (to capture the jet exit velocity of 30m/s) and then to  $500\mu s$  (to capture the low velocity co-flow). The light sheet, coincident with the jet centreline, was approximately 1mm thick.

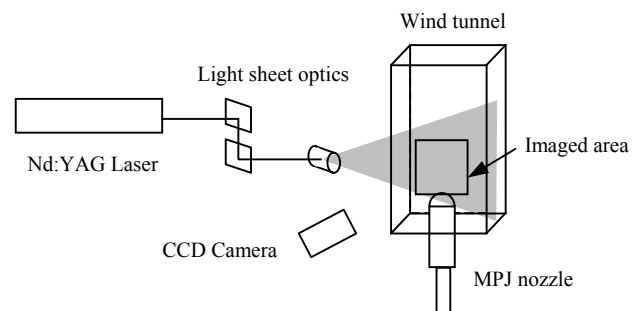


Figure 2. Experimental Apparatus.

The camera used to collect the PIV images was a Kodak Megaplug ES1.0 camera with a CCD array of 1008 (W) x 1018 (H) pixels. This camera has a maximum frame rate of 30 fps, but may be operated in a frame transfer mode, allowing pairs of images to be collected in rapid succession. The first frame has a variable exposure time which may be set between  $1\mu s$  and  $999\mu s$ ; for the present study it was set to  $242\mu s$ . The second frame has a fixed exposure time of 33ms.

The experimental technique was validated using an axisymmetric flow issuing from a smooth contraction.

### PIV Image Analysis

Spatial resolution of the images was determined using a target board featuring graduated markings. The imaged area was 120mm x 120mm in size, to correspond with the area over which Schneider's [12] LDA measurements were performed.

Using this imaged area results in an effective light sheet thickness of approximately 10 pixels. Following PIV interrogation of the MPJ flow, the mean displacement of particles in the radial direction was determined to be approximately 0.5 pixels. The mean azimuthal component of velocity in the MPJ flow is at least 50% smaller than the mean radial component in the near field [12], giving a mean out-of-plane particle displacement of 0.25 pixels, or 2.5% of the light sheet thickness. Thus errors due to out-of-plane motion are considered to be negligible.

It is acknowledged that the area imaged in the current study is not ideal for the particle size used, requiring sub-pixel resolution for truly accurate results. However, this configuration still gives a valid image of the instantaneous velocity field, allowing comparison with previous results. More accurate results may be achieved by decreasing the imaged area.

The PIV images collected were interrogated using cross-correlation of 64 x 64 pixel windows, with an overlap of 50%. The software used was PivView 1.6 (PivTec GmbH, Germany).

## Results and Discussion

The following figures display the results taken at  $f_p=10\text{Hz}$  only, which represents the low Strouhal number ( $St=0.003$ ) MPJ flow. All images are taken at the same phase, that is, when the exiting jet is directed toward the right of the image.

Figure 3 shows a representative instantaneous image of the MPJ flow, with the velocity vector field overlaid. For clarity, the image shown is the negative of the original image. The head of the MPJ nozzle is visible at the bottom of the image, as is the edge of the light sheet. Note that any vectors appearing below the edge of the light sheet are erroneous.

The streaks on either side of the nozzle indicate the strong entrainment of the very low velocity co-flow into the jet fluid. It was determined by Nathan & Luxton [4] that the gross entrainment rate of the fluidic precessing jet (FPJ) over the first three jet exit diameters is five times greater than that of a simple jet.

The vector field of this flow was generated using a time between laser pulses,  $\Delta t$ , of  $50\mu\text{s}$ . This is optimised to capture the jet exit velocity of  $30\text{m/s}$ . Figure 4 shows the velocity field overlaid on contours of the vorticity component normal to the plane of the image. The exiting jet is clearly visible, as is a large scale vortical structure on the left of the image, at an approximate downstream distance of  $x/d_e=4$ . It is important to note that the jet from an MPJ nozzle emerges with negligible tangential motion [12]. However the rotation of the jet about the axis causes the centroid of the emerging jet to form into a helix. Embedded within this helical jet is a counter-rotating vortex pair, somewhat analogous to that of a jet in a cross-flow [8]. Approximately ten diameters downstream from the nozzle (depending upon  $St$ ) the helix has been shown to “merge” or “collapse” so that it forms a shape somewhat analogous to the path of a lasso [8].

Given the helical shape of the emerging jet from an MPJ nozzle, it is clear that the centroid of the emerging jet, shown in figures 3 and 4, will only be in the plane of light sheet at phase angles of  $0^\circ$  (the potential core),  $180^\circ$ ,  $360^\circ$ , etc. The large scale vortex structure on the left side of figures 3 and 4 (centred at about  $r=-40\text{mm}$ ,  $x=60\text{mm}$ ) is deduced to correspond to the slice through the helix at a phase angle of  $180^\circ$ . Paired regions of positive and negative vorticity concentration in this region, visible in figure 4, indicate counter-rotating vortex pairs as described by Schneider

*et al.* [11, 14] and Nobes [8]. Close scrutiny of the data shows low vorticity structures centred at about  $r=50\text{mm}$ ,  $x=80\text{mm}$ , corresponding to the centre of the helix at phase angle of  $360^\circ$ .

The entrained fluid which can clearly be seen to move from the bottom left to the top right of figure 3, can now be interpreted to correspond to the entrainment of ambient air directly into the centre of the helical path of the jet.

The entrainment of ambient fluid into the core of the jet flow described above has important implications for combustion. It provides a path for air to enter the core of the jet upstream from the flame front, quite unlike the case for a simple jet. This air may either promote conditions suitable for stable ignition near to the base of the flame, or may reduce the mixture fraction of the mixed fluid within the flame boundary with possible implications on soot formation.

Consistent with Schneider’s [12] observations of low Strouhal number MPJ flows ( $St=0.002$ ), it can be seen that the deflection of the emerging jet from its initial trajectory of  $45^\circ$  is small. Only negligible deflection from the initial  $45^\circ$  trajectory is observed in the region  $0 < x/d_e < 4$ , based on the downstream position of the large vortical structure indicated in figure 3.

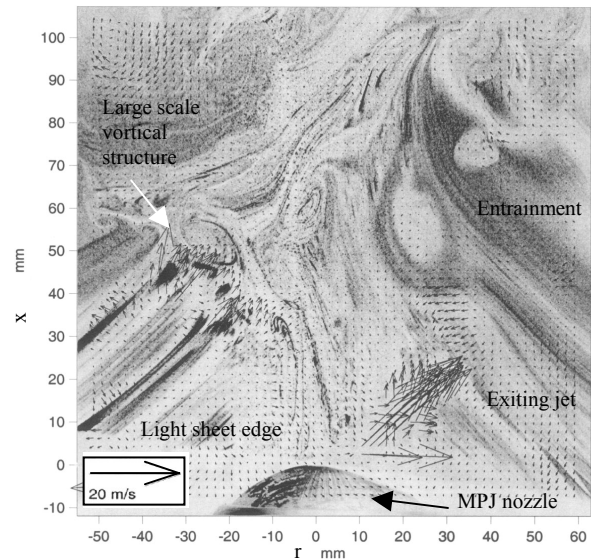


Figure 3. Instantaneous MPJ flow with vector field at  $f_p=10\text{Hz}$ ,  $\Delta t=50\mu\text{s}$ .

In order to resolve the very low velocity regions of the flow, PIV images were also taken for the above flow conditions with the time between laser pulses,  $\Delta t$ , set to  $500\mu\text{s}$ . An instantaneous velocity vector field in this configuration is shown in figure 5. The entrainment of the co-flow into the jet fluid is evident from the inflow of fluid on both vertical boundaries.

Figure 6 shows the normalised axial centreline velocity profile of the low Strouhal number MPJ flow ( $St = 0.003$ ), as determined from two representative instantaneous PIV images, one with  $\Delta t=50\mu\text{s}$  and one with  $\Delta t=500\mu\text{s}$ . The instantaneous profile for  $\Delta t=50\mu\text{s}$  agrees closely with the averaged results obtained by Schneider [12] for  $St=0.002$  (phase-average and ensemble-average), both of which show no recirculation zone along the centreline. However, the new data show smaller axial velocities at  $x/d_e < 4$ . The instantaneous profile for  $\Delta t=500\mu\text{s}$ , which gives improved resolution of the low velocity at the centreline, indicates reverse flow in the region  $0 < x/d_e < 4$ , and broadly agrees with the results of Mi *et al.* [2] for  $St=0.005$  in this region. However, the results of Mi *et al.* [2] show this recirculation zone

extending to  $x/d_e=7$ ; the instantaneous results presented here for  $x/d_e > 4$  instead correlate closely with those obtained by Schneider [12]. Viewing these data collectively, it is evident that the disparity in the existence and size of the recirculation zone may be a function of the precessional Strouhal number, with the size of the recirculation zone increasing with increasing Strouhal number.

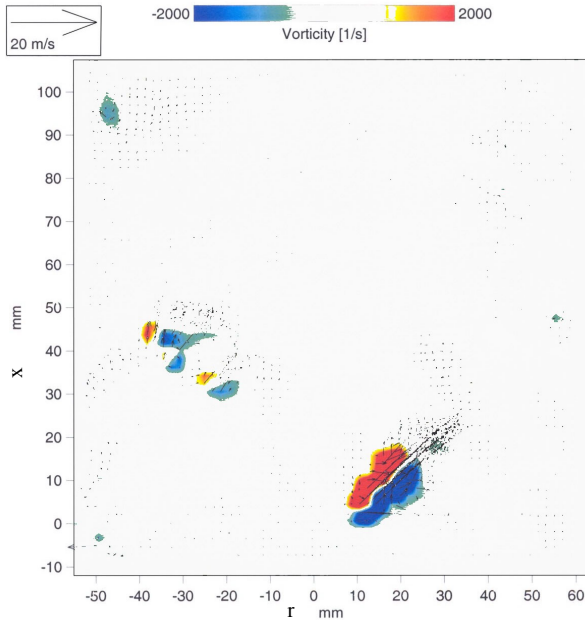


Figure 4. Velocity & vorticity field of the MPJ flow at  $f_p=10\text{Hz}$ ,  $\Delta t=50\mu\text{s}$ .

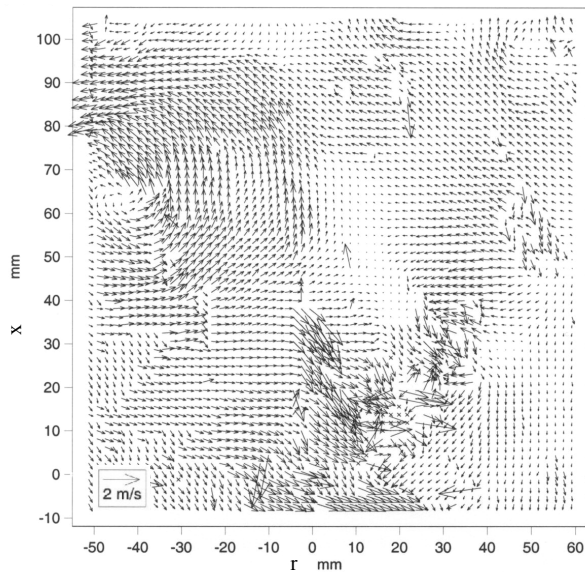


Figure 5. Vector field of the MPJ flow at  $f_p=10\text{Hz}$ ,  $\Delta t=500\mu\text{s}$ .

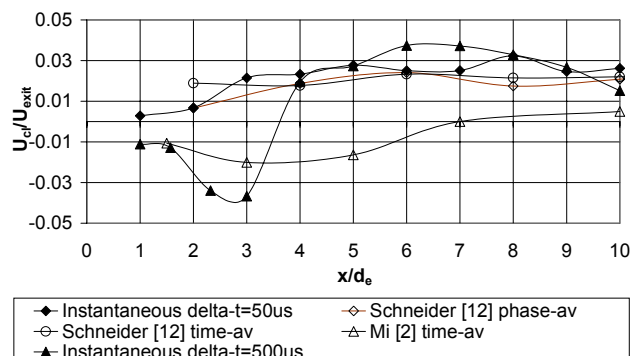


Figure 6. Centreline axial velocity profiles, low St flow.

## Conclusions

These results provide the first detailed instantaneous images of the structure of the flow generated by a mechanical precessing jet at a low Strouhal number. The use of the PIV technique to obtain quantitative data on the flow has been compared against existing data on the MPJ flow and demonstrates strong consistency.

The present study also demonstrates the complexity of obtaining reliable PIV data in flows where very large velocity variations exist. These complexities may be ameliorated by the use of smaller imaged areas which, in turn, will allow improved resolution of the particle locations. The use of the phase-averaging technique is necessary if these individual images are to be assembled into larger flow fields.

## Acknowledgments

The authors acknowledge the financial assistance provided to this project by the Australian Research Council.

The authors also thank Dr Zeyad Alwahabi of the Department of Chemical Engineering, and Mr Chong Yau Wong of the Department of Mechanical Engineering, Adelaide University, Adelaide, for their assistance with the set-up and execution of these experiments.

## References

- [1] Manias, C.J., Nathan, G.J., Low  $\text{NO}_x$  Clinker Production, *J World Cement*, 1994.
- [2] Mi, J., Luxton, R.E., Nathan, G.J., The Mean Flow Field of a Precessing Jet, *13th Australasian Fluid Mechanics Conference*, Melbourne, Australia, 1998.
- [3] Nathan, G.J., *The Enhanced Mixing Burner*, PhD Thesis, Department of Mechanical Engineering, University of Adelaide, Australia, 1988.
- [4] Nathan, G.J., Luxton, R.E., The Entrainment and Combustion Characteristics of an Axi-Symmetric, Self-Exciting, Enhanced Mixing Nozzle, *ASME/JSME Thermal Engineering Proceedings*, 5, 1991, 145-152.
- [5] Nathan, G.J., Luxton, R.E., Mixing Enhancement by a Self-Exciting, Asymmetric Precessing Flow-Field, *Proc. Fourth International Symposium on Transport Phenomena in Heat and Mass Transfer*, Sydney, Australia, 1991, 1297-1307.
- [6] Nathan, G.J., Luxton, R.E., Smart, J.P., Reduced  $\text{NO}_x$  Emissions and Enhanced Large Scale Turbulence from a Precessing Jet Burner, *24th Symposium of Combustion*, Sydney, Australia, 1992.
- [7] Newbold, G.J.R., Nobes, D.S., Alwahabi, Z.T., Nathan, G.J., Luxton, R.E., The Application of PIV to the Precessing Jet Nozzle, *12th Australasian Fluid Mechanics Conference*, Sydney, Australia, 1995.
- [8] Nobes, D.S., *The Generation of Large Scale Structures by Jet Precession*, PhD Thesis, Department of Mechanical Engineering, University of Adelaide, Australia, 1998.
- [9] Nobes, D.S., *The Stanford Report*, Internal Document, Department of Mechanical Engineering, The University of Adelaide, 2000.
- [10] Raffel, M., Willert, C., Kompenhans, J., *Particle Image Velocimetry: A Practical Guide*, Heidelberg; Springer-Verlag, 1998.
- [11] Schneider, G.M., Nathan, G.J., Luxton, R.E., An Experimental Study of a Precessing, Deflected Jet, *Proc. 11th Australasian Fluid Mechanics Conference*, Hobart, Australia, 1992, 1105-1108.
- [12] Schneider, G.M., *Structures and Turbulence Characteristics in a Precessing Jet Flow*, PhD Thesis, Department of Mechanical Engineering, University of Adelaide, Australia, 1996.
- [13] Schneider, G.M., Froud, D., Syred, N., Nathan, G.J., Luxton, R.E., Velocity Measurements in a Precessing Jet Flow using a Three Dimensional LDA System, *Exp. Fluids*, 23, 1997, 89-98.
- [14] Schneider, G.M., Newbold, G.J.R., Nathan, G.J., Luxton, R.E., Vortical Structures in a Turbulent Precessing Jet, *Fourth Conference of Experimental Heat Transfer and Fluid Mechanics*, Brussels, Belgium, 1997.